

---

# Generative Flows with Invertible Attentions

---

Rhea Sanjay Sukthanker<sup>1</sup>, Zhiwu Huang<sup>1</sup>, Suryansh Kumar<sup>1</sup>, Radu Timofte<sup>1</sup>, Luc Van Gool<sup>1,2</sup>

<sup>1</sup>Computer Vision Lab, ETH Zürich, Switzerland <sup>2</sup>PSI, KU Leuven, Belgium  
rhea.sukthanker@inf.ethz.ch, {zhiwu.huang, sukumar, radu.timofte, vangool}@vision.ee.ethz.ch

## Abstract

Flow-based generative models have shown excellent ability to explicitly learn the probability density function of data via a sequence of invertible transformations. Yet, modeling long-range dependencies over normalizing flows remains understudied. To fill the gap, in this paper, we introduce two types of invertible attention mechanisms for generative flow models. To be precise, we propose map-based and scaled dot-product attention for unconditional and conditional generative flow models. The key idea is to exploit split-based attention mechanisms to learn the attention weights and input representations on every two splits of flow feature maps. Our method provides invertible attention modules with tractable Jacobian determinants, enabling seamless integration of it at any positions of the flow-based models. The proposed attention mechanism can model the global data dependencies, leading to more comprehensive flow models. Evaluation on multiple generation tasks demonstrates that the introduced attention flow idea results in efficient flow models and compares favorably against the state-of-the-art unconditional and conditional generative flow methods.

## 1 Introduction

Recent developments in deep generative models have successfully demonstrated their ability to model complex real-world datasets for various applications, such as image synthesis [1–3], image super-resolution [4–6], facial manipulation [7–9], autonomous driving [10, 11], and others. The widely studied modern generative models include generative adversarial nets (GANs) [1, 12, 13], variational autoencoders (VAEs) [2, 14, 15], autoregressive models [16, 17] and flow-based models [18, 3, 19]. The GAN models implicitly learn the data distribution to produce samples by transforming a noise distribution into the desired space, where the generated data can approximate the real data distribution. On the other hand, VAEs optimize a lower bound on the data’s log-likelihood, leading to a suitable approximation of the actual data distribution. Although these two models have achieved great success, neither of them targets direct data distribution learning.

The autoregressive models [21, 16, 17] and the flow-based generative models [3, 18, 19] optimize the exact log-likelihood of the real data. Although autoregressive models perform better on density estimation benchmarks, their sequential property results in non-trivial parallelization. Hence, by comparison, the flow-based generative models are conceptually attractive due to tractable log-likelihood, exact latent-variable inference, and parallelizability of both training and synthesis. Notably, they allow exact inference of the actual data log-likelihood via normalizing flow. As shown in Fig. 1 (a), the normalizing flow model transforms a simple distribution into a complex one by applying a sequence of invertible transformation functions, which leads to an excellent mechanism of simultaneous exact log-likelihood optimization and latent-variable inference. Owing to efficiency constraints on the network design, most flow-based generative models require a large number of flow layers to approximate non-linear long-range data dependencies [22] to get globally coherent samples. To overcome this drawback, modeling the long-range dependencies efficiently over normalizing flows is the key, and presently it is one of the most sought-after problems [20, 22].

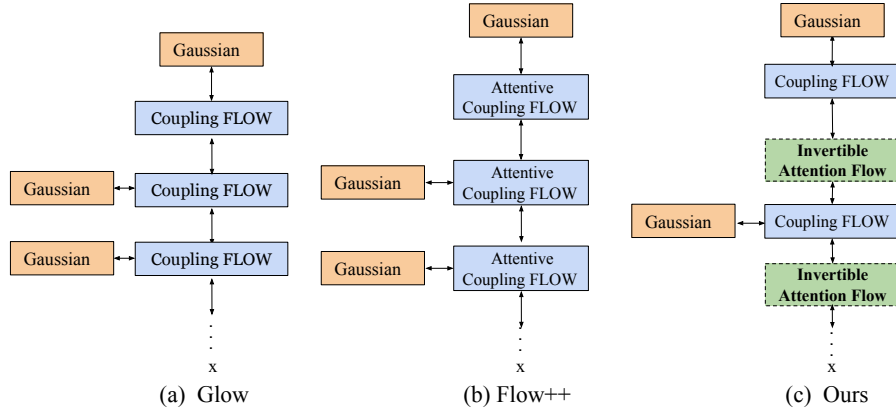


Figure 1: Conceptual comparison of our method (c) against two representative flow-based generative models, i.e., generative flow (Glow) [19] (a) and Flow++ [20] (b). Based on Glow, Flow++ introduces the conventional attention mechanism to model short-term dependencies within one split of each flow feature map in the context of coupling layers. In contrast, our proposed method further introduces invertible attention mechanisms to any flow positions to learn long-term correlations along each entire flow feature maps.

To model long-range dependencies in normalizing flow-based generative models, one may opt to combine multi-scale autoregressive priors [22]. By comparison, exploiting attention mechanisms is an efficient way to model the long-range dependencies for deep learning systems. It imitates human brain actions of selectively concentrating on a few relevant information while ignoring other less correlated ones. Traditional self-attention mechanisms like [23–25] exhibit a good balance between the ability to model long-range dependencies and the computational and statistical efficiency. In general, the self-attention modules measure the response at a point as a weighted sum of the features at all points, where the attention weights are computed at a small computational cost. Although [20] recently applied the conventional attention directly as a dependent component in the coupling layer (Fig.1 (b)), it learns dependency within a short-range (i.e., one split of each flow feature map) of the coupling layer. To our knowledge, the domain of learning the long-range dependencies over normalizing flows is understudied. A natural solution is to exploit new attention mechanisms which can be applied to learn any long-range correlations of the feature maps at any positions of the invertible flow-based models. However, it is generally non-trivial to achieve that goal of exploiting new attention modules as independent flow layers. Concretely, such attention should also maintain the invertibility property with tractable Jacobian determinants in the flow-based generative model.

In this paper, we propose an invertible attention mechanism that can model long-range dependencies and can be introduced at any position of the flow-based models (along the entire flow feature maps, see Fig.1 (c)). The key idea is to leverage our check-board masking strategy for the two-split generation, with which the attention weights and the attention input representation can be administered separately. Such a computation strategy can make the attention modules invertible and the corresponding Jacobian determinants tractable and hence, can be integrated seamlessly into any flow models. Notably, we exploit two different invertible attention mechanisms to encode the first- and second-order long-term correlations respectively in the context of flow feature maps. The two proposed attention mechanisms are 1) *invertible map-based (iMap) attention* that explicitly models the first-order correlations among the flow feature maps, 2) *invertible scaled dot-product (iSDP) attention* that explicitly models the second-order long-range interactions among distant positions in the attention dimension. Since the two attention modules explicitly model the dependencies of flow features maps, it further enhances a flow-based model’s ability to represent the long-term dependencies. To show the competence of our approach, we evaluated the introduced attention models in the context of both unconditional and conditional flow-based generative models for image generation and image super-resolution task. Statistical performances clearly demonstrate the benefit of our method.

## 2 Related Work

**Generative Flows.** Early flow-based generative models like [3, 26, 18, 27] are introduced for exact inference of real data log-likelihood. They are generally constructed by a sequence of invertible transformations to map a base distribution to a complex one.

In recent years, various unconditional generative flow models like [19, 28, 20, 22] have been emerging to extend the early flow models to multi-scale architectures with split couplings that allow for efficient inference and sampling. For instance, [19] additionally introduces invertible  $1 \times 1$  convolutions to encode non-linearity in the data distribution for the unconditional setup. [29] introduces more general  $d \times d$  invertible convolutions to enlarge the receptive field. [28] exploits residual blocks of flow layers (*i.e.*, a flexible family of transformations) where only Lipschitz conditions rather than strict architectural constraints are needed for enforcing invertibility. [20] improves the coupling layer with variational dequantization, continuous mixture cumulative distribution function, and self-attention. The self-attention is applied directly to the intrinsic neural function of the coupling layer. Because of the nature of the affine coupling layer, attention is not required to be invertible. Besides, this direct attention application merely learns the dependencies within one of the two splits of channel-wise flow dimensions, and thus its receptive field is greatly limited. In contrast, our introduced attention is an independent flow layer that should be invertible and can learn more general and longer-range dependencies across different splits of flow feature maps. In other words, [20] models within-split dependencies while ours learns cross-split correlations, and hence both are complementary for each other. More recently, [22] models channel-wise dependencies through multi-scale autoregressive priors. The introduced dependency modeling is limited on latent space, and hence it can be complementary to our exploited attentions on intermediate flow dimensions.

On the other hand, recent conditional flow models like [30–33, 6] have also been explored, aiming at conditional image synthesis. For instance, [30] exploits two invertible networks for source and target and a relation network that maps the latent spaces to each other. In this way, conditioning information can be leveraged at the appropriate hierarchy level and hence, can overcome the restriction of always using raw images as input. Similarly, [32] exploits a parallel sequence of invertible mappings in which a source flow guides the target flow at every step. [33] additionally introduces conditioning networks that allow all operations in the target-domain flow conditioned on the source-domain information. For better conditioning, [6] exploits conditional affine coupling layers that accept the source domain’s features map extracted by one external neural network as the conditions. For more direct information transfer from the source domain, [6] introduces a conditional affine injector that directly feeds the conditions to all channels and spatial locations in activation maps. To our knowledge, these conditional generative flow models rarely learn long-term dependencies.

**Attention Models.** To address the problem of missing global information in convolutional operations, attention mechanisms like [23, 34, 35, 24, 36, 25, 37] have emerged as a recent advance to model long-distance interactions. In particular, self-attention generally calculates the response at a position in a sequence by attending to all positions within the same sequence, which allows for long-range interactions without increasing the number of parameters. For example, [38, 39, 25] introduce map-based attention to improve the performance of convolutional networks on image recognition, where spatial attention maps are learned to scale the features given by convolutional layers. [23] integrates the scaled dot-product attention along with its multi-head versions into an auto-encoder, which has become the de-facto standard for natural language processing tasks. [34, 24] exploit non-local blocks that can be viewed as one single dot-product attention to capture long-range dependencies in images and videos for either image generation or video classification. More recently, [37] studies that a pure transformer applied directly to sequences of image patches can perform very well on image classification tasks. Despite this progress, attention mechanisms have rarely been explored in the context of the flow-based generative models, where each neural operation is constrained to preserve tractability of the inverse and Jacobian determinant computation.

### 3 Overview and Background

This paper introduces two invertible attention mechanisms to learn the long-range dependencies for unconditional and conditional flow-based generative models<sup>1</sup>. The long-distance interaction modeling is capable of producing more efficient flow models. Below we provide an overview of the unconditional and conditional generative flow models, followed by an outline of the proposed attention mechanisms.

In the *unconditional flow* setup, the generative flows aim at learning invertible transformations (*i.e.*,  $f_\theta, g_\theta$ , where  $\mathbf{z} = f_\theta(\mathbf{x}) = g_\theta^{-1}(\mathbf{x})$  with model parameters  $\theta$ ) between a simple distribution

<sup>1</sup>Our paper focuses on studying invertible flows that allow for both efficient exact inference and sampling.

Table 1: STEPOFFLOW layers for either unconditional or conditional flow models used as our backbones [22, 6]. Here  $\mathbf{x}$ ,  $\mathbf{c}$ ,  $\mathbf{y}$  indicate input, condition and output respectively, and SPLIT, NN denote the split operation and the regular neural network operations respectively.

Layer	Function	Layer	Function
Actnorm	$\forall i, j : \mathbf{y}_{i,j} = \mathbf{s} \odot \mathbf{x}_{i,j} + \mathbf{b}$	Invertible $1 \times 1$ convolution	$\forall i, j : \mathbf{y}_{i,j} = \mathbf{W} \mathbf{x}_{i,j}$
Affine coupling	$\mathbf{x}_a, \mathbf{x}_b = \text{SPLIT}(\mathbf{x})$ $(\log \mathbf{s}, \mathbf{t}) = \text{NN}(\mathbf{x}_b)$ $\mathbf{y}_a = \exp(\log \mathbf{s}) \odot \mathbf{x}_a + \mathbf{t}$ $\mathbf{y} = (\mathbf{y}_a, \mathbf{x}_b)$	Mixture affine coupling	$\mathbf{x}_a, \mathbf{x}_b = \text{SPLIT}(\mathbf{x})$ $(\log \mathbf{s}, \mathbf{t}, \pi, \mu, \log \hat{\mathbf{s}}) = \text{NN}(\mathbf{x}_b)$ $\mathbf{y}_a = \sigma^{-1}(f(\mathbf{x}_a, \pi, \mu, \log \hat{\mathbf{s}})) \odot \exp(\log \mathbf{s}) + \mathbf{t}$ $\mathbf{y} = (\mathbf{y}_a, \mathbf{x}_b)$ , where $f(\mathbf{x}_a, \pi, \mu, \log \hat{\mathbf{s}}) := \sum_i \pi_i \sigma((x - \mu_i) \odot \exp(-\log \hat{\mathbf{s}}_i))$
Conditional affine coupling	$\mathbf{x}_a, \mathbf{x}_b = \text{SPLIT}(\mathbf{x})$ $(\log \mathbf{s}, \mathbf{t}) = \text{NN}(\mathbf{x}_b, \mathbf{c})$ $\mathbf{y}_a = \exp(\log \mathbf{s}) \odot \mathbf{x}_a + \mathbf{t}$ $\mathbf{y} = (\mathbf{y}_a, \mathbf{x}_b)$	Conditional affine injector	$(\log \mathbf{s}, \mathbf{t}) = \text{NN}(\mathbf{c})$ $\mathbf{y} = \exp(\log \mathbf{s}) \odot \mathbf{x} + \mathbf{t}$

$\mathbf{z} \sim p_\theta(\mathbf{z})$  and a complex one  $\mathbf{x} \sim p_\theta(\mathbf{x})$ . The function  $f_\theta$  (and, likewise,  $g_\theta$ ) are parameterized by an invertible neural network, consisting of a sequence of  $L$  invertible functions  $f_{\theta_i}$ . Hence, the network model is typically called as a (normalizing) flow:  $f_\theta = f_{\theta_1} \circ f_{\theta_2} \circ \dots \circ f_{\theta_L}$ , mapping the simple distribution density on the latent variable  $\mathbf{z}$  to the complex distribution density on the data  $\mathbf{x}$ :

$$\mathbf{x} \xleftarrow{f_{\theta_1}} \mathbf{h}_1 \xleftarrow{f_{\theta_2}} \mathbf{h}_2 \dots \xleftarrow{f_{\theta_L}} \mathbf{z}. \quad (1)$$

Given the log-likelihood of  $p_\theta(\mathbf{z})$ , the change of variables formula enables us to compute the log-likelihood of the data  $\mathbf{x}$  under the transformation  $f_\theta$ :

$$\log p_\theta(\mathbf{x}) = \log p_\theta(\mathbf{z}) + \log |\det \partial \mathbf{z} / \partial \mathbf{x}| = \log p_\theta(f_\theta(\mathbf{x})) + \sum_{i=1}^L \log |\det \partial \mathbf{h}_i / \partial \mathbf{h}_{i-1}|, \quad (2)$$

where  $\partial \mathbf{h}_i / \partial \mathbf{h}_{i-1}$  is the Jacobian of the invertible transformation  $f_{\theta_i}$  moving from  $\mathbf{h}_{i-1}$  to  $\mathbf{h}_i$  with  $\mathbf{h}_0 \equiv \mathbf{x}$ . The scalar value  $\log |\det J_{\theta_i}|$  is the log-determinant of the Jacobian matrix<sup>2</sup>. The likelihood of  $p_\theta(\mathbf{z})$  is commonly modeled as Gaussian likelihood, *e.g.*,  $p(\mathbf{z}) = \mathcal{N}(\mathbf{z} | \mu, \sigma)$ . The exact likelihood computation allows us to train the network by minimizing the negative log-likelihood (NLL) loss.

In the *conditional flow* setting, the invertible neural network  $f_\theta$  maps the input data-condition pair  $(\mathbf{x}, \mathbf{c})$  to a latent variable  $\mathbf{z} = f_\theta(\mathbf{x}; \mathbf{c})$ . Here, the data  $\mathbf{x}$  can be exactly reconstructed from the latent encoding  $\mathbf{z}$  conditioning on  $\mathbf{c}$  as  $\mathbf{x} = f_\theta^{-1}(\mathbf{z}; \mathbf{c})$ . The log-likelihood of the data  $\mathbf{x}$  can be computed as

$$\log p_\theta(\mathbf{x} | \mathbf{c}) = \log p_\theta(f_\theta(\mathbf{x}; \mathbf{c})) + \sum_{i=1}^L \log |\det \partial \mathbf{h}_i / \partial \mathbf{h}_{i-1}|, \text{ where } \mathbf{h}_i = f_{\theta_i}(\mathbf{x}; \mathbf{c}) \quad (3)$$

For both the unconditional and conditional flow models, the design of flow layers generally respects the protocol that computing the inverse and Jacobian determinant of the involved transformations  $f_{\theta_i}$  should be tractable. In this paper, we employ [22] and [6] as two of our backbones for unconditional and conditional flow models respectively. In both of the two backbones, the flow network is organized into  $L$  flow-levels, each operating at a resolution containing  $K$  number of flow-steps. In practice, each flow-level  $f_{\theta_i}$  is typically composed of SQUEEZE, STEPOFFLOW, and SPLIT operations. SQUEEZE trades off spatial resolution for channel dimension. STEPOFFLOW is commonly a series of affine coupling layers, invertible  $1 \times 1$  convolutions and normalization layers. SPLIT divides an intermediate layer  $h_i$  into two halves, one of which will be transformed and the other of which will be left unchanged. Table 1 summarizes the functions of the major layers of STEPOFFLOW.

To explicitly model the long-range dependencies for better flow models, we study two types of invertible attention mechanisms: (1) *invertible map-based (iMap) attention*: It aims at learning a

<sup>2</sup>In general, flow-based generative models choose those transformations whose Jacobian is a triangular matrix for tractable computation of log-determinants.

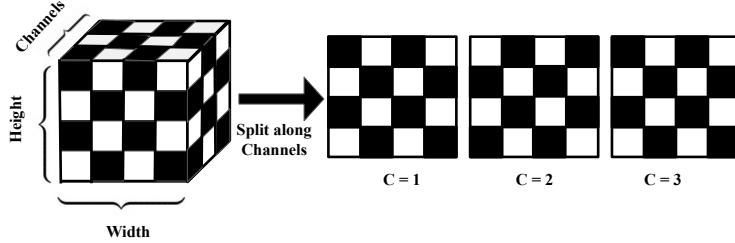


Figure 2: Checkboard masking scheme for invertible attentions. The 3D masking aims for globally permuted binary patterns (i.e., a two-split generation,  $x_1, x_2$ ) on the whole feature flow maps, which better facilitates the production of invertible attention layers.

weighting factor for each position in the attention dimension and scales the flow feature maps with the learned attention weights. Such attention is expected to model the first-order long-term dependencies among the flow dimensions explicitly. (2) *invertible scaled dot-product (iSDP) attention*: It computes the representation response at a position as a weighted sum of features of all the positions along the attention dimension. The attention weights are computed by scaled dot-product between features of all the positions. Compared to the iMap attention, it explicitly models the second-order long-range dependencies among the distant positions along the attention dimension.

## 4 Proposed Attention Flow

The proposed attention flow (AttnFlow) aims at inserting invertible map-based (iMap) and scaled dot-product attention (iSDP) flow layers to conventional flow-based generative models (see Fig.1 (c)), so that different types of long-range correlations can be learned to enhance the representation power of normalizing flows. Like conventional attention mechanisms, an attention operation accepts a feature map  $\mathbf{h}_{in}$  of shape  $(H, W, C_{in})$  as input, and outputs an attended featured map  $\mathbf{h}_{out}$  of shape  $(H, W, C_{out})$  with a transformation  $\mathbf{h}_{out} = G(\mathbf{h}_{in})$ . In practice, attention learning consists of three steps: (1) reshaping the input feature map  $\mathbf{h}_{in}$ , (2) computing the attention weights  $\mathbf{W}_{attn}$ , and (3) applying the learned attention weights to output  $\mathbf{h}_{out}$ . To accommodate the introduced attention modules into normalizing flows, we should also ensure the attention transformation  $G$  preserve the tractability of inverse and Jacobian determinant computation. For this purpose, we introduce a 3D checkboard masking strategy for globally permuted binary patterns (i.e., two-split generation  $x_1, x_2$ ) of the entire flow feature maps. Our strategy is inspired by the existing split techniques as proposed in [18, 19]. Fig.2 illustrates the suggested checkboard masking scheme. The permutation is first performed on the whole space (along the domains of height, width, and channels) of the input feature maps, and then the binary split is conducted along the channels. Compared to the masking strategies in [18, 19], ours is able to generate binary patterns globally and thus leads to longer-range learning on attentions. The simple nature of the introduced global split better ensures the involved attention can be invertible easily (see Fig.7 for the computation graph of forward and inverse propagation of our further introduced attentions). Further, the resulting Jacobian, in this case, is a block-lower-triangular matrix whose determinant can be computed easily using the product of the determinants of the diagonal block matrices. Below we provide the details of the two introduced invertible attentions, their inverse propagation, and the corresponding Jacobian determinant computation.

**iMap Attention.** The major idea of iMap is to scale the feature map with the learned attention weights based on the first-order correlations of flow dimensions. Concretely, we study the iMap attention mechanism over the spatial domain of flow feature maps. Mathematically, the attention weights can be calculated as

$$\mathbf{W}_{imap} = G_5((1 - \mathbf{M})G_4(G_3(G_2(G_1(\mathbf{h}_{in})))) + \mathbf{M}\mathbf{b}), \quad (4)$$

where  $\mathbf{M}$  is a 2D checkboard mask,  $\mathbf{b}$  is a learnable variable,  $G_1(\mathbf{h}_{in}) = \mathbf{M}\mathbf{h}_{in}$ ,  $G_2$  is a 1D convolutional layer with kernel size as 1, which reduces the dimension of the feature response of each channel from  $C_{in}$  to  $C'$ , and outputs a feature map of shape  $(H \times W, C')$ . Without loss of generality,  $G_3$  applies average pooling<sup>3</sup> to each channel dimensions and outputs an  $(H \times W)$ -dim vector for spatial attention learning. The operator  $G_4$  is to reorganize the  $(H \times W)$  attention weights into a

<sup>3</sup>Performing average pooling over the spatial domain turns to learn channel attention, provided the spatial resolution for train and validation are same.

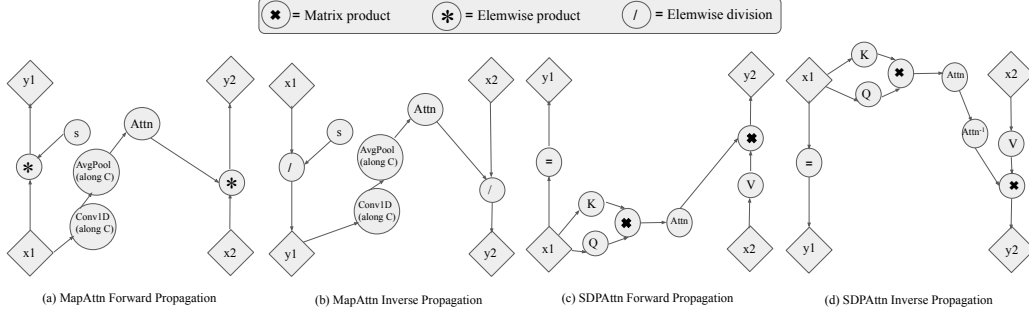


Figure 3: Computational graph of forward and inverse propagation of the proposed Map-based (a)(b) and SDP-based (c)(d) attention mechanisms. Due to the simple nature of the introduced split-based strategy, the involved attentions are both easily invertible and possesses a tractable Jacobian determinant. In (a,b),  $s$  is a learnable scale parameter, and the average pooling is performed along channels for spatial attention learning. In (c,d),  $K, Q, V$  are the three basic elements for the iSDP attention. They are computed by regular  $1 \times 1$  2D convolutions within the masking scheme, which allows for invertible operations.

$(H \times W) \times (H \times W)$  matrix, where the attention weights of shape  $(H \times W)$  are placed on the diagonal of the matrix. The derived attention weight matrix  $\mathbf{W}_{\text{imap}}$  is a diagonal matrix. The function  $G_5$  corresponds to standard activation functions such as softmax and sigmoid. Finally, we apply the attention weight matrix  $\mathbf{W}_{\text{imap}}$  to the input feature map through matrix multiplication to obtain the attended feature map  $\mathbf{h}_{\text{out}} = \mathbf{W}_{\text{imap}} \mathbf{h}_{\text{in}}$ . The forward and inverse propagation of AttenFlow-iMap module is illustrated in Fig.7 (a,b). The Jacobian determinant of the introduced iMap transformation is computed as follows:

$$\frac{\partial \mathbf{h}_{\text{in}}}{\partial \mathbf{h}_{\text{out}}} = \sum (\mathbf{M} \log(G_5(\mathbf{b})) + \sum (\frac{HW}{2} \log(G_5(G'(\mathbf{h}_{\text{in}}))))), \quad (5)$$

where  $G_5$  indicates the corresponding activation function,  $G'(\mathbf{h}_{\text{in}}) = G_3(G_2(G_1(\mathbf{h}_{\text{in}})))$ ,  $G_1, G_2, G_2$  are masking, 1D convolution and average pooling respectively, which are mentioned before.

**iSDP Attention.** The conventional SDP attention is originally from [23]. The success of this attention mainly stems from the effective learning of long-term second-order correlations among involved feature maps and the exploitation of three different representations for attention learning. The attention function can be expressed as mapping a query  $\mathbf{q}_{\text{in}}$  and a set of key-value  $(\mathbf{k}_{\text{in}}, \mathbf{v}_{\text{in}})$  pairs to an output  $\mathbf{h}_{\text{out}}$ . The query and the key are employed to learn the second-order attention weights through a scaled dot-product computation, which is further applied to the input value for the final attended output.

To introduce the SDP attention to the flow models, as shown in Fig.7 (c), we apply two invertible  $1 \times 1$  2D convolutions to the input feature map to obtain a query-key pair  $(\mathbf{q}_{\text{in}}, \mathbf{k}_{\text{in}})$ , and use the input feature maps to play the role of the value  $\mathbf{v}_{\text{in}}$ . The attention is applied between patches of the input following [37]. In particular, the whole input is split into  $N$  patches and the iSDP attention is applied to the image patch-wise. The primary goal is to capture the inter-patch interaction with the attention weights. In practice, we compute the attention function on a set of queries simultaneously, packed together into a matrix  $\mathbf{Q}$ . The keys and values are also packed together into matrices  $\mathbf{K}$  and  $\mathbf{V}$ . Below formulates the mapping process:

$$\mathbf{h}_{\text{out}} = \mathbf{W}_{\text{isdsp}} \mathbf{V} = G_4\left(\frac{\mathbf{Q}\mathbf{K}^T}{\sqrt{d}}\right) \mathbf{V} \quad (6)$$

where  $\mathbf{Q} = G_2(G_1(\mathbf{h}_{\text{in}}))$ ,  $\mathbf{K} = G_3(G_1(\mathbf{h}_{\text{in}}))$ ,  $\mathbf{V} = G_1(\mathbf{h}_{\text{in}})$ ,  $G_1(\mathbf{h}_{\text{in}}) = \mathbf{M}\mathbf{h}_{\text{in}}$  (here  $\mathbf{M}$  is a 2D checkboard mask),  $G_2, G_3$  correspond to two regular  $1 \times 1$  2D convolutions,  $G_4$  corresponds to the activation function.  $G_2, G_3$  are computed within the introduced masking, which allows for invertible operations. In general, dot-product values often get large to influence the final negative log-likelihood scales. Hence, inspired by [23], we apply  $d$  to scale the dot-product values. For a better scaling, we make  $d$  learnable. Fig.7 (d) demonstrates the inverse propagation of the introduced iSDP attention, which can be computed easily.

The Jacobian of the proposed iSDP transformation is a lower block triangular matrix, with the attention weights  $\mathbf{W}_{\text{isdsp}}$  forming the (repeated) block diagonal entries. As the determinant of a lower

block triangular matrix is simply the product of determinants of the matrices along the diagonal, the Jacobian determinant of iSDP can be computed as

$$\frac{\partial \mathbf{h}_{\text{in}}}{\partial \mathbf{h}_{\text{out}}} = \prod (\det(\frac{P}{2} \mathbf{W}_{\text{isdP}})), \quad (7)$$

where  $P$  is the patch size, *i.e.*, the feature dimension within each patch.

## 5 Experimental Evaluation

In this section, we evaluate the proposed unconditional and conditional attention flow (AttnFlow, cAttnFlow) models for image generation and image super-resolution respectively. In addition, we present more experimental details and evaluations in the supplementary material.

**Image Generation.** We use two standard benchmark datasets (*i.e.*, MNIST [40] and CIFAR10 [41]).

**1) AttnFlow Setup.** The proposed AttnFlow can be applied to any off-the-shelf unconditional generative flow models that generally need attentions. For the image generation task, we employ the architecture of the state-of-the-art flow (mARFlow)<sup>4</sup> [22] as the backbone of AttnFlow, where our proposed iMAP and iSDP attention flow layers can be inserted. Each level of mARFlow sequentially stacks an actnorm layer, an invertible  $1 \times 1$  convolution layer, and a coupling layer. Specially, [22] applies a mixture cumulative distribution function as well as an internal attention module to the coupling layer. Under the mARFlow backbone, we inserted our proposed attention modules (either iMap or iSDP) into one of the following four positions: 1) Before actnorm (pos-1), 2) after actnorm (pos-2), 3) after invertible convolution (pos-3), and 4) after coupling (pos-4). To study AttnFlow’s efficiency, we evaluate its various setups on the numbers of flow-levels, flow-steps, and channels. Regarding the hyperparameter setup, we use Adamax with a learning rate of  $8 \times 10^{-4}$ , as done in [22, 19]. Besides, we follow [22, 20] to utilize a batch size of 32 for both MNIST and CIFAR10. We use Sigmoid for the activation function, and empirically set the patch number  $N = 4$  for iSDP.

**2) Competing Methods.** We compare four state-of-the-art unconditional generative flow models, including Glow [19], Flow++ [20], Residual Flow [28] and mARFlow [22]. Note that our AttnFlow’s architecture is based on mARFlow with coupling layers closest to Glow. By comparison, Flow++ does not include the SPLIT operation, and uses a different uniform dequantization. Hence, the comparison with Glow and mARFlow serves as a better ablation to measure the effectiveness and efficiency of our AttnFlow. For a reference, we also compare one representative GAN model, *i.e.*, deep convolutional GAN (DCGAN) [42].

**3) Comparison.** We summarize the quantitative results of our AttnFlows and the competing methods on MNIST and CIFAR10 in Table 2 and Table 3. We use the per-pixel log-likelihood metric in bits/dims for both MNIST and CIFAR10. Additionally, we employ three more standard metrics, *i.e.*, Fréchet Inception Distance (FID) [43], inception scores [44] and Kernel Inception Distance (KID) [45], to measure the generated sample quality on CIFAR10. From the results in Table 2 and Table 3, we can see that both of our AttnFlow-iMap and AttnFlow-iSDP can clearly outperform the backbone mARFlow with similar model complexities (*i.e.*, the same level and step numbers), and our AttnFlows can achieve better results than the other state-of-the-art flow models. Furthermore, our lighter model (with a smaller number of steps or a smaller channel) typically achieve comparable performances (or even better results) compared to those heavier mARFlow models. The comparison in Fig.10 also shows the proposed model generates more visually pleasing samples.

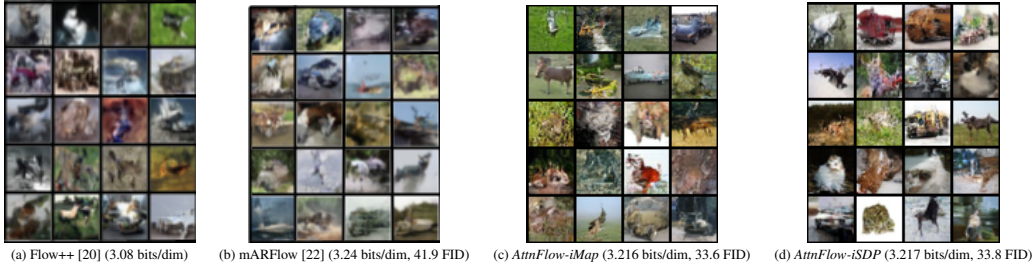


Figure 4: Comparison of samples from the proposed model with state-of-the-art models on CIFAR10.

<sup>4</sup>We employ mARFlow’s official code: <https://github.com/visinf/mar-scf/>

Table 2: Evaluation of sample quality on MNIST. \* indicates the result reported in the mARFlow paper [22]. As MNIST is a small dataset and very complex model is not at all required, the performance gets decreased when our model’s complexity increases. (**Bold**: best, Underline: second best)

Method	Levels	Steps	Channels	Parameters (MB)	bits/dim ( $\downarrow$ )
Glow [19]	3	32	512	–	1.05
Residual Flow [28]	3	16	–	–	0.97
mARFlow [22]	3	4	96	46.01	0.56 (0.88*)
<i>AttnFlow-iMap</i>	3	4	96	46.03	0.43
<i>AttnFlow-iSDP</i>	3	4	96	46.25	0.44
<i>AttnFlow-iMap</i>	3	2	96	23.78	0.41
<i>AttnFlow-iSDP</i>	3	2	96	23.89	0.42
<i>AttnFlow-iMap</i>	3	2	48	8.94	<b>0.39</b>
<i>AttnFlow-iSDP</i>	3	2	48	9.05	<u>0.40</u>

Table 3: Evaluation of sample quality on CIFAR10. Note that \* indicate the results for the ICML workshop version of mARFlow [22]. (**Bold**: best, Underline: second best)

Method	Level	Step	Channel	Parameter (MB)	bits/dim ( $\downarrow$ )	FID ( $\downarrow$ )	Incep ( $\uparrow$ )	KID ( $\downarrow$ )
DCGAN [42]	–	–	–	–	–	37.1	6.4	–
Glow [19]	3	32	512	–	3.35	46.9	–	–
Flow++ [20]	3	–	96	–	3.29	46.9	–	–
Residual Flow [28]	3	16	–	–	3.28	46.3	5.2	–
mARFlow [22]	3	4	96	46.01	3.27 (3.254*)	(40.5*)	(5.8*)	(0.033*)
mARFlow [22]	3	4	256	252.77	3.24 (3.222*)	41.9 (33.9*)	5.7 (6.5*)	(0.026*)
<i>AttnFlow-iMap</i>	3	4	96	46.03	3.247	40.5	6.0	0.031
<i>AttnFlow-iSDP</i>	3	4	96	46.25	3.248	40.2	5.9	0.032
<i>AttnFlow-iMap</i>	3	4	256	252.79	<b>3.216</b>	<b>33.6</b>	<u>6.6</u>	<b>0.025</b>
<i>AttnFlow-iSDP</i>	3	4	256	253.01	<u>3.217</u>	<u>33.8</u>	<b>6.7</b>	<b>0.025</b>

**Image Super-Resolution.** We follow [6] to use the splits of the CelebA dataset [46] for image super-resolution (SR). Specifically, we use the full train split of CelebA for the training high-resolution (HR) image set, and employ 5000 images from the test split of CelebA to test the HR images.

**1) cAttnFlow Setup.** Our conditional AttnFlow (cAttnFlow) is based on the architecture of the state-of-the-art super-resolution flow (SRFlow)<sup>5</sup> [6] model. The flow network is organized into  $L = 4$  flow-levels, each of which operate a specific resolution of  $H/2^l \times W/2^l$  ( $H \times W$ ,  $L$  indicate the resolution of HR images and the  $l$ -th flow-level respectively). Each flow-level is composed of  $K$  flow-steps. Each flow-step stacks four different layers: 1) Acnorm, 2)  $1 \times 1$  invertible convolution, 3) affine injector, and 4) conditional affine layers. As done for image generation, we also insert our proposed attentions after the existing flow layers in each level of SRFlow.

**2) Competing Methods.** Following [6], we compare with bicubic and the state-of-the-art SR methods, including ESRGAN [5] and SRFlow [6]. As we use SRFlow as our cAttnFlow’s backbone, the comparison with it can help us focus on improvement using our introduced attention mechanisms.

**3) Comparison.** Table 4 reports the comparison of our cAttnFlow against the competing methods in terms of four standard metrics, including SSIM, PSNR, LR-PSNR [6] and LPIPS [47]. The results imply that our model can achieve the best balance among the four used metrics compared to the competing methods. The improvements of our cAttnFlow over the backbone SRFlow are visible at two different level model complexities, showing that our introduced attention is able to enhance the efficiency of the flow models. Fig.5 also shows the visual comparison.

**Ablation Study.** As shown in Fig.6, we ablate the proposed attention models on 1) different attention positions, and 2) different head numbers. We generally observe that inserting the attention layers in the position after the permutation layer (pos-3) and after the coupling layer (pos-4) are the most favourable positions. On the other hand, the use of more than 3 attention heads does not provide a significant performance improvement.

<sup>5</sup>We utilize SRFlow’s official code at <https://github.com/andreas128/SRFlow/>



Table 4: Results for  $8\times$  SR on CelebA. We report average SSIM, PSNR, LR-PSNR and LPIPS scores for SRFlow and ours at different temperatures (0.1-0.9). (**Bold**: best, Underline: second best)

Method	Levels	Steps	Parameters (MB)	SSIM ( $\uparrow$ )	PSNR ( $\uparrow$ )	LR-PSNR ( $\uparrow$ )	LPIPS ( $\downarrow$ )
Bicubic	–	–	–	0.63	23.15	35.19	0.58
ESRGAN [5]	–	–	–	0.63	22.88	34.04	<b>0.12</b>
SRFlow [6]	1	1	6.622	0.67	<b>25.57</b>	44.20	0.23
SRFlow [6]	2	8	13.25	<u>0.73</u>	25.47	38.94	0.17
<i>cAttnFlow-iMap</i>	1	1	6.623	0.71	<u>25.50</u>	<b>44.75</b>	0.19
<i>cAttnFlow-iSDP</i>	1	1	6.630	<u>0.73</u>	<u>25.50</u>	<u>44.23</u>	0.18
<i>cAttnFlow-iMap</i>	2	8	13.30	<b>0.74</b>	25.38	41.88	0.17
<i>cAttnFlow-iSDP</i>	2	8	13.93	<u>0.73</u>	25.24	42.49	<u>0.16</u>

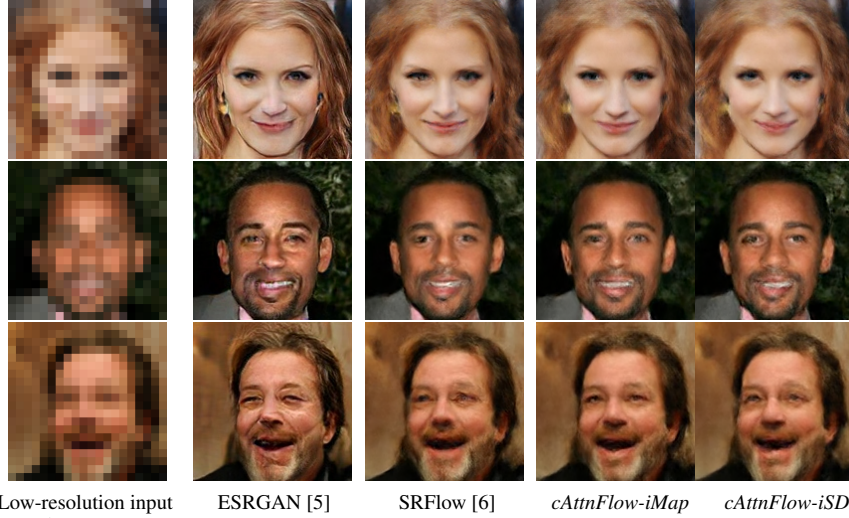


Figure 5: Comparison of the proposed AttnFlow with state-of-the-art for  $8\times$  face SR on CelebA.

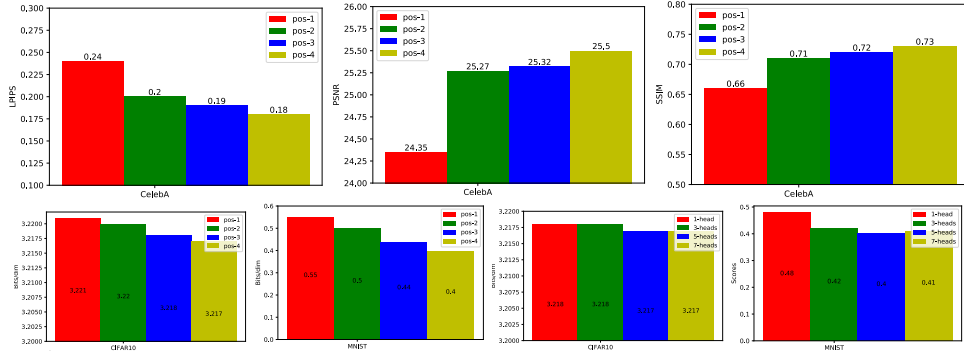


Figure 6: Ablation studies of the proposed attentions on different positions in the flow layers (pos-1: before actnorm, pos-2: after actnorm, pos-3: after permutation, pos-4: after coupling layer) and different number of attention heads for the iSDP attention (1h: 1head, 3h: 3 head, 5h: 5 head). For better visualization, see suppl.

## 6 Conclusion and Future Work

This paper introduces two invertible attention modules for both the unconditional and conditional generative flow models. The proposed attention is capable of learning long-range dependencies and hence highly strengthens the representation efficiency of the flow-based generative models. Our experimental evaluation on image generation and super-resolution show the clear improvement of our proposed attention over the used unconditional and conditional flow-based backbones.

One of our model’s major limitations lies in its unsatisfactory scaling ability to deeper flows. For example, it is non-trivial to apply our attention to the full SRFlow model that contains more flow levels. Following the study in [48], one of the most promising solutions is to introduce residual learning to avoid the attention vanishing problem in the context of deeper invertible flow models.

## Acknowledgments

This work was supported in part by the ETH Zürich Fund (OK), an Amazon AWS grant, and an Nvidia GPU grant. Suryansh Kumar’s project is supported by “ETH Zürich Foundation and Google, Project Number: 2019-HE-323” for bringing together best academic and industrial research.

## References

- [1] Goodfellow, I. J.; Pouget-Abadie, J.; Mirza, M.; Xu, B.; Warde-Farley, D.; Ozair, S.; Courville, A.; Bengio, Y. Generative adversarial networks. NIPS. 2014.
- [2] Kingma, D. P.; Welling, M. Auto-encoding variational bayes. ICLR. 2014.
- [3] Dinh, L.; Krueger, D.; Bengio, Y. NICE: Non-linear independent components estimation. ICLR Workshop. 2015.
- [4] others., et al. Photo-realistic single image super-resolution using a generative adversarial network. CVPR. 2017.
- [5] Wang, X.; Yu, K.; Wu, S.; Gu, J.; Liu, Y.; Dong, C.; Loy, C. C.; Qiao, Y.; Tang, X. ESRGAN: Enhanced Super-Resolution Generative Adversarial Networks. ECCV. 2018.
- [6] Lugmayr, A.; Danelljan, M.; Van Gool, L.; Timofte, R. SRFlow: Learning the super-resolution space with normalizing flow. ECCV. 2020.
- [7] Huang, R.; Zhang, S.; Li, T.; He, R. Beyond face rotation: Global and local perception gan for photorealistic and identity preserving frontal view synthesis. ICCV. 2017.
- [8] Choi, Y.; Choi, M.; Kim, M.; Ha, J.-W.; Kim, S.; Choo, J. Stargan: Unified generative adversarial networks for multi-domain image-to-image translation. CVPR. 2018.
- [9] Pumarola, A.; Agudo, A.; Martinez, A. M.; Sanfeliu, A.; Moreno-Noguer, F. Ganimation: Anatomically-aware facial animation from a single image. ECCV. 2018.
- [10] Wang, E.; Cui, H.; Yalamanchi, S.; Moorthy, M.; Djuric, N. Improving Movement Predictions of Traffic Actors in Bird’s-Eye View Models using GANs and Differentiable Trajectory Rasterization. SIGKDD. 2020.
- [11] Zhang, M. Y.; Huang, Z.; Paudel, D. P.; Thoma, J.; Van Gool, L. Weakly Paired Multi-Domain Image Translation. BMVC. 2020.
- [12] Brock, A.; Donahue, J.; Simonyan, K. Large Scale GAN Training for High Fidelity Natural Image Synthesis. ICLR. 2018.
- [13] Karras, T.; Laine, S.; Aila, T. A style-based generator architecture for generative adversarial networks. CVPR. 2019.
- [14] Makhzani, A.; Shlens, J.; Jaitly, N.; Goodfellow, I.; Frey, B. [arXiv preprint arXiv:1511.05644](https://arxiv.org/abs/1511.05644) **2015**,
- [15] Tolstikhin, I.; Bousquet, O.; Gelly, S.; Schölkopf, B. Wasserstein Auto-Encoders. ICLR. 2018.
- [16] van den Oord, A.; Kalchbrenner, N.; Espeholt, L.; Kavukcuoglu, K.; Vinyals, O.; Graves, A. Conditional Image Generation with PixelCNN Decoders. NIPS. 2016.
- [17] Van Oord, A.; Kalchbrenner, N.; Kavukcuoglu, K. Pixel recurrent neural networks. ICML. 2016.
- [18] Dinh, L.; Sohl-Dickstein, J.; Bengio, S. Density estimation using real nvp. ICLR. 2017.
- [19] Kingma, D. P.; Dhariwal, P. Glow: Generative Flow with Invertible 1x1 Convolutions. NeurIPS. 2018.
- [20] Ho, J.; Chen, X.; Srinivas, A.; Duan, Y.; Abbeel, P. Flow++: Improving flow-based generative models with variational dequantization and architecture design. ICML. 2019.

- [21] Domke, J.; Karapurkar, A.; Aloimonos, Y. Who killed the directed model? CVPR. 2008.
- [22] Mahajan, S.; Bhattacharyya, A.; Fritz, M.; Schiele, B.; Roth, S. Normalizing flows with multi-scale autoregressive priors. CVPR. 2020.
- [23] Vaswani, A.; Shazeer, N.; Parmar, N.; Uszkoreit, J.; Jones, L.; Gomez, A. N.; Kaiser, L.; Polosukhin, I. Attention is All you Need. NIPS. 2017.
- [24] Zhang, H.; Goodfellow, I.; Metaxas, D.; Odena, A. Self-attention generative adversarial networks. ICML. 2019.
- [25] Wang, X.; Xiong, X.; Neumann, M.; Piergiovanni, A.; Ryoo, M. S.; Angelova, A.; Kitani, K. M.; Hua, W. Attentionnas: Spatiotemporal attention cell search for video classification. ECCV. 2020.
- [26] Kingma, D. P.; Salimans, T.; Jozefowicz, R.; Chen, X.; Sutskever, I.; Welling, M. Improved Variational Inference with Inverse Autoregressive Flow. NIPS. 2016.
- [27] Papamakarios, G.; Pavlakou, T.; Murray, I. Masked autoregressive flow for density estimation. NIPS. 2017.
- [28] Chen, R. T.; Behrmann, J.; Duvenaud, D.; Jacobsen, J.-H. Residual Flows for Invertible Generative Modeling. NeurIPS. 2019.
- [29] Hooeboom, E.; Van Den Berg, R.; Welling, M. Emerging convolutions for generative normalizing flows. ICML. 2019.
- [30] Sun, H.; Mehta, R.; Zhou, H. H.; Huang, Z.; Johnson, S. C.; Prabhakaran, V.; Singh, V. Dual-glow: Conditional flow-based generative model for modality transfer. ICCV. 2019.
- [31] Lu, Y.; Huang, B. Structured output learning with conditional generative flows. AAAI. 2020.
- [32] Pumarola, A.; Popov, S.; Moreno-Noguer, F.; Ferrari, V. C-flow: Conditional generative flow models for images and 3d point clouds. CVPR. 2020.
- [33] Sorkhei, M.; Henter, G. E.; Kjellström, H. arXiv preprint arXiv:2012.05846 **2020**,
- [34] Wang, X.; Girshick, R.; Gupta, A.; He, K. Non-local neural networks. CVPR. 2018.
- [35] Xu, T.; Zhang, P.; Huang, Q.; Zhang, H.; Gan, Z.; Huang, X.; He, X. Attngan: Fine-grained text to image generation with attentional generative adversarial networks. CVPR. 2018.
- [36] Bello, I.; Zoph, B.; Vaswani, A.; Shlens, J.; Le, Q. V. Attention augmented convolutional networks. ICCV. 2019.
- [37] others,, et al. arXiv preprint arXiv:2010.11929 **2020**,
- [38] Park, J.; Woo, S.; Lee, J.-Y.; Kweon, I. S. BAM: Bottleneck Attention Module. BMVC. 2018.
- [39] Woo, S.; Park, J.; Lee, J.-Y.; Kweon, I. S. Cbam: Convolutional block attention module. ECCV. 2018.
- [40] LeCun, Y.; eon Bottou, L.; Bengio, Y.; Haffner, P. PROC. OF THE IEEE **1998**,
- [41] others,, et al. Technical report **2009**,
- [42] Radford, A.; Metz, L.; Chintala, S. Unsupervised representation learning with deep convolutional generative adversarial networks. ICLR. 2016.
- [43] Heusel, M.; Ramsauer, H.; Unterthiner, T.; Nessler, B.; Hochreiter, S. Gans trained by a two time-scale update rule converge to a local nash equilibrium. NIPS. 2017.
- [44] Salimans, T.; Goodfellow, I. J.; Zaremba, W.; Cheung, V.; Radford, A.; Chen, X. Improved Techniques for Training GANs. NIPS. 2016.
- [45] Bińkowski, M.; Sutherland, D. J.; Arbel, M.; Gretton, A. Demystifying MMD GANs. ICLR. 2018.

- [46] Liu, Z.; Luo, P.; Wang, X.; Tang, X. Deep learning face attributes in the wild. ICCV. 2015.
- [47] Zhang, R.; Isola, P.; Efros, A. A.; Shechtman, E.; Wang, O. The Unreasonable Effectiveness of Deep Features as a Perceptual Metric. CVPR. 2018.
- [48] Dong, Y.; Cordonnier, J.-B.; Loukas, A. [arXiv preprint arXiv:2103.03404](https://arxiv.org/abs/2103.03404) **2021**,
- [49] Cordts, M.; Omran, M.; Ramos, S.; Rehfeld, T.; Enzweiler, M.; Benenson, R.; Franke, U.; Roth, S.; Schiele, B. The Cityscapes Dataset for Semantic Urban Scene Understanding. 2016.
- [50] Isola, P.; Zhu, J.-Y.; Zhou, T.; Efros, A. A. Image-to-image translation with conditional adversarial networks. Proceedings of the IEEE conference on computer vision and pattern recognition. 2017; pp 1125–1134.

## Supplementary Material

The following supplementary document includes: (A) Neural architecture design illustration of the proposed attention flows (AttnFlows), (B) detailed experimental setup, (C) training details and curves, (D) more visual results on MNIST, CIFAR10 and CelebA, (E) an evaluation on a new backbone for image translation on Cityscapes, (F) better visualization plots of the ablation study presented in the main paper on the three used datasets, as well as some more results for different iSDP-based attention head numbers on CelebA, (G) pseudo code of the proposed key components (i.e., iMap and iSDP), and (H) further remarks on the possible future directions.

### A AttnFlow Network Architecture

The proposed attention flow model (AttnFlow) aims to insert invertible map-based (iMap) and scaled dot product-based (iSDP) attentions to regular flow-based generative models. Fig.7 (a) (b) show the neural architecture design of regular flow-based generative models and the proposed AttnFlow respectively. As shown in (b), the invertible attention modules (i.e., iMap and iSDP) can be stacked on the affine coupling layers. It is also possible to add the attention modules at any other positions, such as before invertible  $1 \times 1$  convolution, or actnorm. The detailed architectures of the proposed iMap and iSDP are illustrated in Fig. 7 (c) (d) respectively. Their designs follow the conceptual graphs of forward and inverse propagation of the proposed Map-based and SDP-based attention mechanisms that are shown in Fig.3 of the major paper. In particular, both of the iMap and iSDP modules apply the 3D checkboard mask in order to make the proposed attention invertible. After the 3D masking, the iMap attention further applies map-based transformations (i.e., 1D convolution and average pooling) for the first-order attention learning. By comparison, the iSDP attention aims at learning the second-order correlations among the flow feature maps with a scaled dot-product over two different transformations of inputs, which are obtained by two 2D convolutions, respectively. More architecture details of the iMap and iSDP are demonstrated in Fig.7 (c) (d).

### B Detailed Experimental Setup

We used MNIST [40], CIFAR10 [41] and CelebA [46] datasets to evaluate the proposed AttnFlows in the main paper. MNIST is a dataset of 70,000 small square  $28 \times 28$  pixel grayscale images of handwritten single digits between 0 and 9. Following most of the generative modeling works such as [19, 22], we use the whole dataset from the real set to train our AttnFlows and the competing methods. CIFAR10 dataset is comprised of 60,000  $32 \times 32$  pixel color images of objects from 10 classes, such as frogs, birds, cats, ships, airplanes, etc. To train the proposed AttnFlows and its competitors, we also utilize the whole dataset for the real data. We additionally evaluate the proposed cAttnFlows for face super-resolution ( $8\times$ ) using 5000  $160 \times 160$  images from the test split of the CelebA dataset. Following [6], we apply a bicubic kernel to down-scale those selected images into  $20 \times 20$  low-resolution images. We use 162770 training images following the same setup as [6] for the train-test split. In the supplementary paper, we additionally use Cityscapes [49] to evaluate our models. Each data instance of this dataset is a picture of a street scene that is segmented into objects of 30 different classes, e.g., road, sky, buildings, cars, and pedestrians. 5000 of these images come with fine per-pixel class annotations of the image, and this is commonly called as segmentation masks.

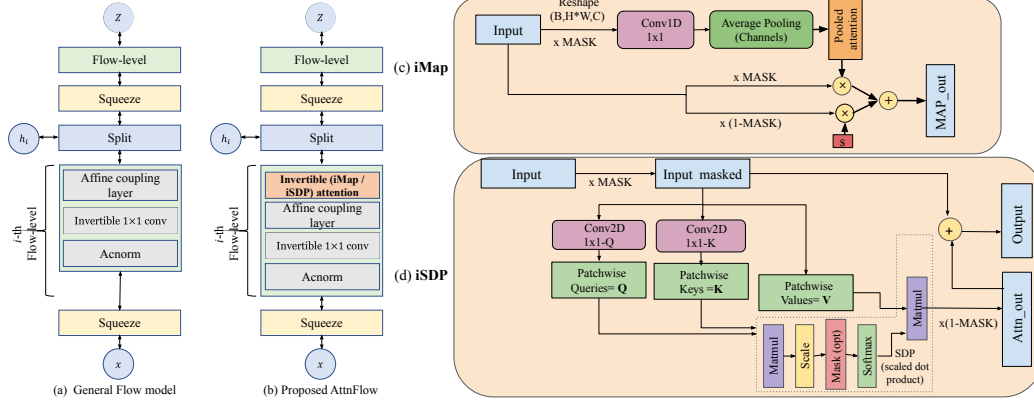


Figure 7: (a) Neural architecture of regular flow-based generative models. (b) Neural architecture design of the proposed attention flow model (AttnFlow), which aims at inserting invertible map-based (iMap) and scaled dot product-based (iSDP) attentions to regular flow-based generative models.  $\mathbf{x}$ ,  $\mathbf{h}_i$ ,  $\mathbf{z}$  indicates the data, latent variable and intermediate coding respectively.  $B$ ,  $H$ ,  $W$ ,  $C$  indicate batch size, image height, width, and channel number respectively.  $\times$  MASK represents the masking operation that applies 3D checkboard mask to the input. Conv2D  $1 \times 1$  is an invertible 2D convolution.  $s$  is a learnable scale. Finally averaged pooled features are fed with learnable parameters into  $\text{MAP}_{\text{out}}$  that is sigmoid function. (d) Detailed design of iSDP. MASK indicates the 3D checkboard masking, and Mask(opt) is optional.

We employ the data splits provided by the original dataset (2975 training and 500 validation images), and train different models to generate street-scene images conditioned on their segmentation masks.

## C Training Details and Curves

A single TITAN-RTX GPU (24GB) is used to train each of the proposed AttnFlows/cAttnFlows. Specially, the batch size is set to 32 for the training on them on both of MNIST and CIFAR10. The proposed AttnFlow-iMap models are trained for around 2 and 3 days for the MNIST and CIFAR10 datasets respectively. On the other hand, the proposed AttnFlow-iSDP models are trained for about 3 and 5 days respectively. The number of iterations for convergence are 100k iterations and 90k iterations for MNIST and CIFAR10 respectively. The proposed cAttnFlow-iMap ( $L=2, K=8$ ) is trained for 3 days, and cAttnFlow-iSDP is trained for 4 days on the CelebA datasets. A batch size is fixed as 16 for all the models on CelebA. The number of steps for convergence are 500k iterations for all the models. On the Cityscapes dataset, cAttnFlow-iMap ( $L=2, K=8$ ) is trained for 2 days, and cAttnFlow-iSDP is trained for 3 days. A batch size is set to 1 for all the models due to the memory limit. The number of steps for convergence are 200k iterations for all the models on Cityscapes.

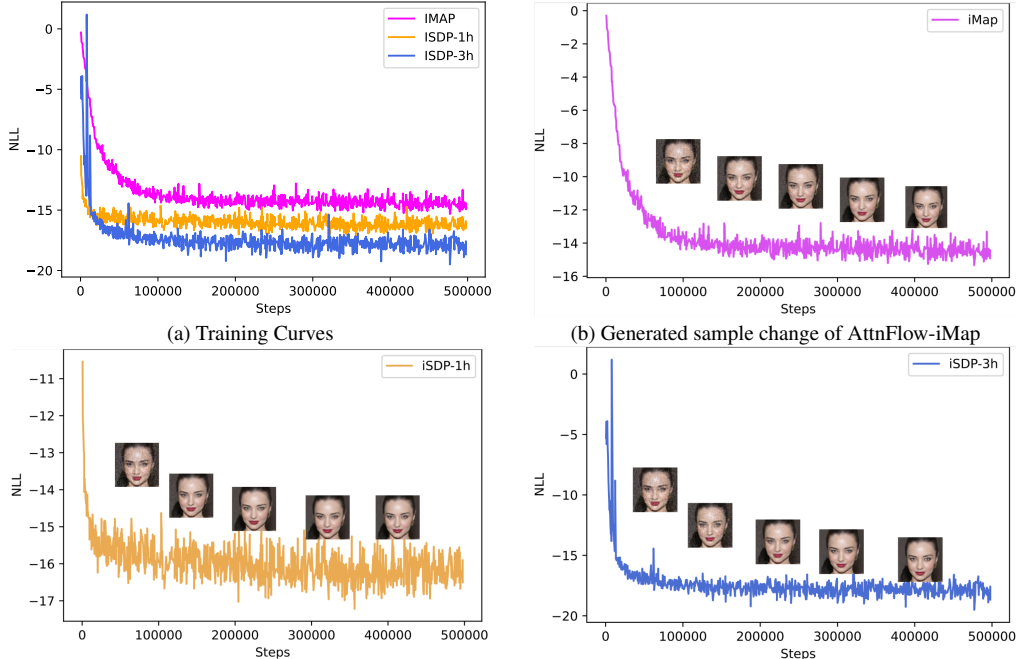
Fig.8 (a) shows the training curves of the proposed AttnFlow-iMap and AttnFlow-iSDP on CelebA. It reflects that the proposed AttnFlows can be trained smoothly for a good convergence in terms of the negative log-likelihood (NLL) loss. In addition, Fig.8 (b)(c)(d) demonstrate the sample change along the training processes of the proposed AttnFlows. They show that the generated samples can keep improving the quality until the convergence.

## D More Results for MNIST, CIFAR10 and CelebA

Fig.9, Fig.10 and Fig.11 show more visual results of the proposed AttnFlows and the competing methods on MNIST, CIFAR10 and CelebA respectively. From the results, we can observe that the generated samples of our proposed AttnFlows are highly competitive, and some are more visually pleasing compared to the competing methods.

## E Evaluation on a New Backbone for Image Translation

We additionally reports the evaluations from applying the proposed models to the image translation task on Cityscapes [49], where segmentation label images are translated into RGB images.



(a) Training Curves (b) Generated sample change of AttnFlow-iMap  
(c) Generated sample change of AttnFlow-iSDP (1 head) (d) Generated sample change of AttnFlow-iSDP (3 heads)

Figure 8: (a) Training curves of the proposed AttnFlow-iMap and AttnFlow-iSDP (with 1, 3 head(s)) on CelebA. The x axis corresponds to the training iterations, and the y axis indicates the negative log-likelihood (NLL) values. (b-d) Generated sample change along the training process of AttnFlow-iMap and AttnFlow-iSDP (with 1, 3 head(s)), showing that the generated sample keeps improving the quality until the model converges.

**1) cAttnFlow Setup.** Our conditional AttnFlow (cAttnFlow) is based on the state-of-the-art conditional flow (Full-Glow)<sup>6</sup> [6] model. The flow network is organized into  $L = 2$  flow-levels, each of which operate a specific resolution of  $H/2^l \times W/2^l$ , where  $H \times W$  indicates the resolution of input images and the  $l$ -th flow-level respectively. Each flow-level is composed of  $K = 8$  flow-steps. Note that our model is much smaller than the original Full-Glow model that consists of 4 levels and each contains 16 steps (i.e.,  $L = 4, K = 16$ ). Each flow-step stacks four different layers: 1) Acnorm, 2)  $1 \times 1$  invertible convolution, 3) affine injector, and 4) conditional affine layers. As done for image generation, we also insert our proposed attentions after the existing flow layers in each level of the Full-Glow model.

**2) Competing Methods.** Following [33], we compare with the state-of-the-art conditional flow methods, C-Glow [31], Dual-Glow [30], and Full-Glow [33]. We also compare the GAN model (Pix2Pix) [50] for a reference. As we use Full-Glow as our cAttnFlow’s backbone, we will focus on the comparison with it, which can clearly show the improvement using our introduced attention mechanisms.

**3) Comparison.** For likelihood-based models, we follow [33] to measure the conditional bits per dimension,  $-\log_2 p(\mathbf{x}_b|\mathbf{x}_a)$ , as a metric of how well the conditional distribution learned by the model matches the real conditional distribution, when tested on held-out examples. Table 5 summarizes the results of the proposed cAttnFlows and its competitors. The comparison shows that the proposed cAttnFlows can achieve better performances than the state-of-the-art conditional flow models. In particular, the proposed cAttnFlows are about  $5 \times$  lighter than their backbone model (Full-Glow), showing that the proposed attention can highly enhance the efficiency of flow models. Besides, the visual comparison in Fig.12 demonstrates that the generated samples of our proposed cAttnFlows are more realistic-looking (particularly richer textures) than those generated by the competing methods.

<sup>6</sup>We utilize Full-Glow’s official code at <https://github.com/MoeinSorkhei/glow2>

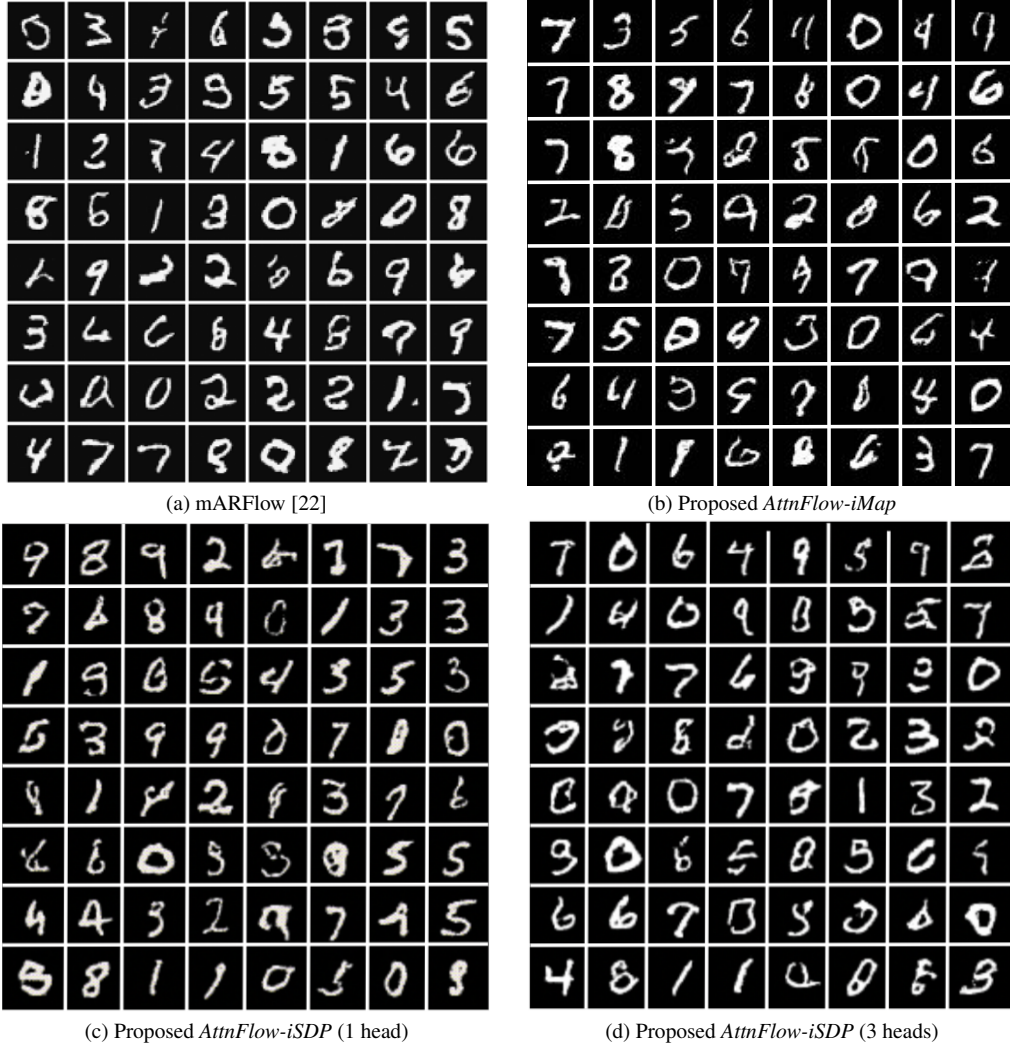


Figure 9: Random samples generated by the proposed AttnFlows and the state-of-the-art flows on the MNIST dataset.

Table 5: Quantitative results of the proposed AttnFlow and the state-of-the-art models on the Cityscapes dataset for label  $\rightarrow$  photo image translation. (**Bold**: best, Underline: second best)

Method	Levels	Steps	Parameters (MB)	Conditional bits/dim ( $\downarrow$ )
C-Glow v.1 [31]	–	–	–	2.568
C-Glow v.2 [31]	–	–	–	2.363
Dual-Glow [30]	–	–	–	2.585
Full-Glow [33]	4	16	155.33	2.345
<i>cAttnFlow-iMap</i>	2	8	34.68	<b>2.310</b>
<i>cAttnFlow-iSDP</i>	2	8	34.70	<u>2.314</u>

## F More Ablation Study

For the ablation study on the proposed AttnFlows, better visualizations of the major paper’s Fig.6 are shown in Fig.13 and Fig.14 . Additionally, Fig.14 includes the ablation study on different head numbers of the proposed AttnFlow-iSDP for CelebA. As shown in Fig.13, inserting the attention modules after each coupling layer generally works the best in the most of cases. Besides, Fig.14 shows that using 5 heads performs the best on the MNIST and CIFAR10 datasets, while employing 3 heads works the best on CelebA. This implies that using 3 or 5 heads is sufficient for the proposed AttnFlow-iSDP on the three employed datasets.

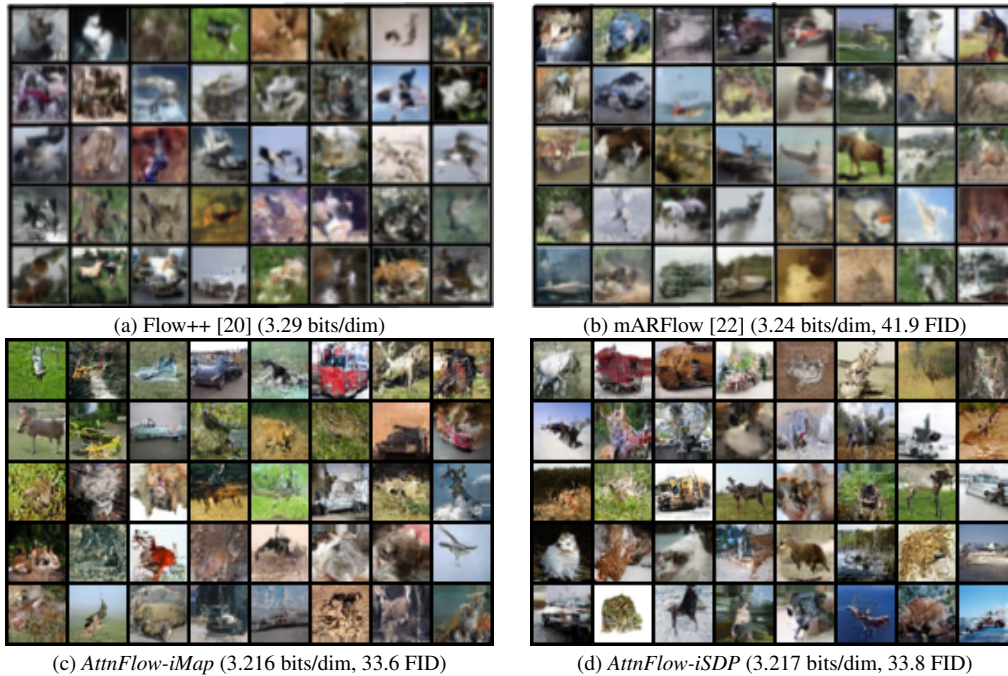


Figure 10: Random samples generated by the proposed AttnFlows and the state-of-the-art flows on the CIFAR10 dataset.

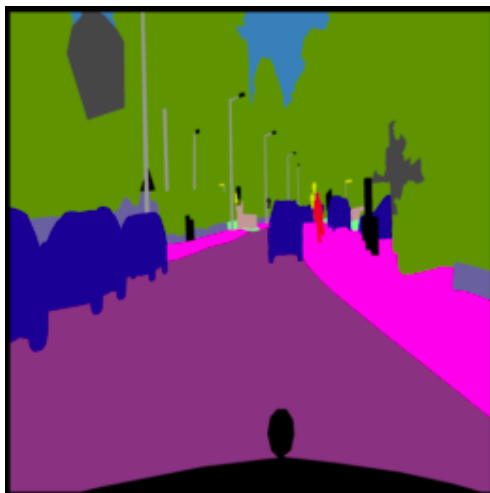


Low-resolution input    ESRGAN [5]    SRFlow [6]    *cAttnFlow-iMap*    *cAttnFlow-iSDP*  
 Figure 11: Super-resolved samples of the proposed *cAttnFlows* and the state-of-the-art models for  $8\times$  face SR on the CelebA dataset.

## G Pseudo Code of Proposed AttnFlows

The proposed *AttnFlow-iMap* and *AttnFlow-iSDP* are built upon the off-the-shelf flow models. Therefore, the major new implementation is on the proposed *iMap* and *iSDP* modules. The pseudo codes for their PyTorch implementation are illustrated in Fig.15.





(a) Input



(b) Pix2PixGAN [50]



(c) Dual-Glow [30]



(d) Full-Glow [33]



(e) Proposed *cAttnFlow-iMAP*



(f) Proposed *cAttnFlow-iSDP*

Figure 12: Generated samples of the proposed *cAttnFlows* and the state-of-the-art models for image translation on the Cityscapes dataset. The competing methods and ours are conditioned on the semantic segmentation labels (a) to synthesize the RGB images with the resolution being of  $256 \times 256$ .

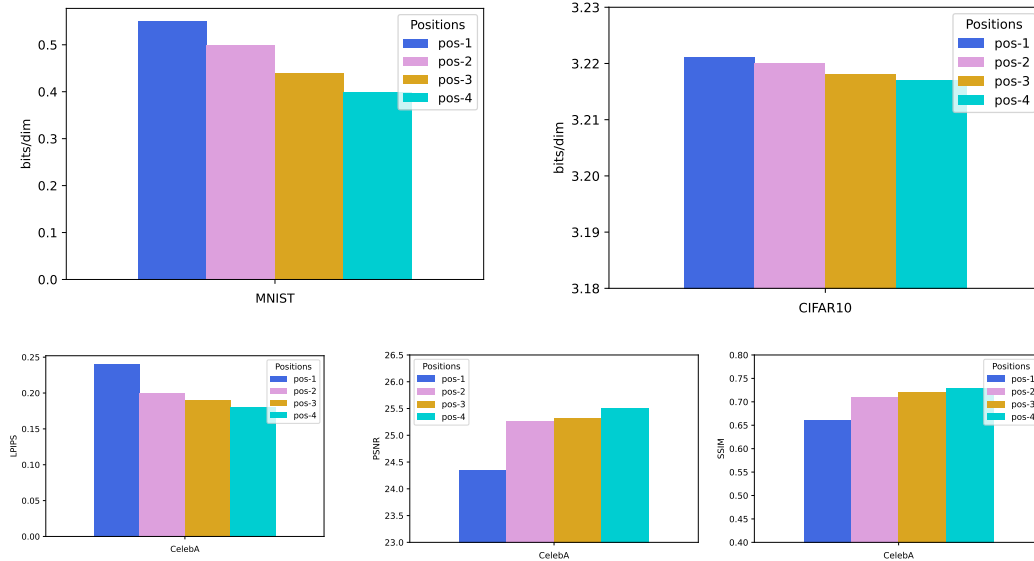


Figure 13: (Better visualisation for Fig.6 in the major paper) Ablation studies of the proposed attentions on different positions in the flow layers (pos-1: before actnorm, pos-2: after actnorm, pos-3: after permutation, pos-4: after coupling layer) on the MNIST, CIFAR10 and CelebA datasets. The Bits/dims metric is employed for MNIST and CIFAR10 (top), and LPIPS, PSNR and SSIM scores are reported on CelebA (bottom).

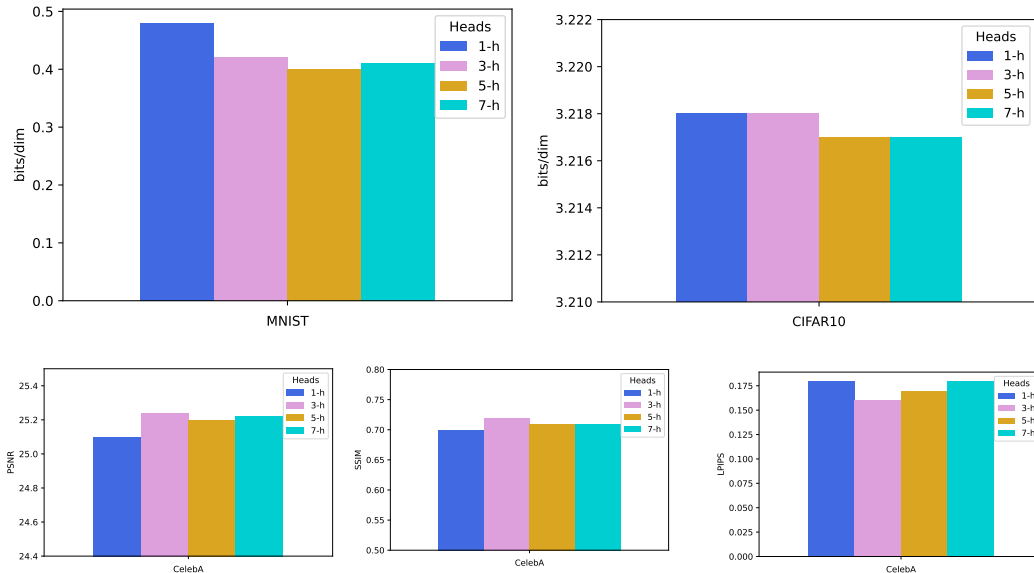


Figure 14: (Better visualisation for Fig.6 in the major paper) Ablation studies of the proposed attentions on different number of attention heads for the proposed iSDP attention (1h: 1head, 3h: 3 heads, 5h: 5 heads, 7h: 7 heads) on the MNIST, CIFAR10 and CelebA datasets. The Bits/dims metric is employed for MNIST and CIFAR10 (top), and LPIPS, PSNR and SSIM scores are reported on CelebA (bottom).

## H Further Remarks for the Future Work

As discussed in the main paper, it is non-trivial to apply the proposed AttnFlows to deeper flows, such as the full SRFlow model that contains more flow levels. We study that it is mainly because the proposed attentions' inverse and Jacobian determinant computations are often numerically unstable when meeting deeper flows. This is roughly matched with the discovery in [48], which finds pure attentions typically lose rank doubly exponentially with the network depth. Inspired by [48], a natural solution is to apply residual learning that is capable of addressing the deep attention problem. In addition, the comprehensive evaluations over the four used datasets show that the proposed AttnFlow-iMap sometimes outperforms AttnFlow-iSDP, while the former also performs worse in some cases.

```

class IMap(nn.Module):
    def __init__(self, input_channels):
        super(IMAP, self).__init__()
        self.input_channels=input_channels
        self.weight = torch.empty([self.input_channels,self.input_channels,1])
        nn.init.kaiming_uniform_(self.weight, a=math.sqrt(5))
        self.weight=torch.nn.Parameter(self.weight).cuda()
        self.bias = torch.empty([self.input_channels])
        fan_in, _ = nn.init.calculate_fan_in_and_fan_out(self.weight)
        bound = 1 / math.sqrt(fan_in)
        nn.init.uniform_(self.bias, -bound, bound)
        self.bias =torch.nn.Parameter(self.bias).cuda()
        self.register_parameter("s",nn.Parameter(torch.randn([1,self.input_channels,1])))
        self.register_parameter("offset",nn.Parameter(torch.ones([1])*8))
        self.pool1 = torch.nn.AvgPool1d(self.input_channels)

    def forward(self, input: torch.Tensor, logdet=0, reverse=False, permute=False):
        if not reverse:
            self.num_channels=input.shape[-1]**2
            self.mask_checkerboard
            B, C, H, W = input.shape
            sig = torch.nn.Sigmoid()
            input_masked = input.view(B, C, H * W) * self.mask
            z = Conv1D(input_masked, self.weight, bias=self.bias) #Conv1d
            z_new = z.transpose(1, 2)
            pool_out = self.pool1(z_new) #Average pooling
            attn_out = (sig(pool_out.squeeze(-1)+self.offset)+1e-5).unsqueeze(1)
            attn_mask = (1 - self.mask) * attn_out + self.mask * (sig(self.s)+1e-5)
            out_new = input * attn_mask.view(B, C,H * W).view(B, C, H, W)
            logdet = logdet + torch.sum((self.input_channels// 2) * (torch.log(sig(pool_out.squeeze(-1)+self.offset)+1e-5)),dim=-1)
            logdet = logdet + torch.sum(torch.log(sig(self.s)+1e-5) * self.mask)
            return out_new,logdet
        else:
            out_new=input
            self.num_channels=input.shape[-1]**2
            self.mask_checkerboard
            B, C, H, W = out_new.shape
            sig = torch.nn.Sigmoid()
            s_sig = sig(self.s)+1e-5
            s_sig_in = torch.ones_like(s_sig) / s_sig
            inp_masked = out_new.view(B, C,H * W) * self.mask * s_sig_in
            out_conv = Conv1D(inp_masked, self.weight, bias=self.bias) #Conv1d
            pool_out = self.pool1(out_conv.transpose(1, 2)) # average pooling
            attn_out = (sig(pool_out.squeeze(2)+self.offset)+1e-5).unsqueeze(1)
            attn_mask = torch.ones_like(attn_out) / attn_out
            attn_mask = (1 - self.mask) * attn_out + self.mask * s_sig_in
            input_rev = out_new * (attn_mask.view(B, C,H * W).view(B, C, H, W))
            logdet = logdet - torch.sum((self.input_channels// 2) * (torch.log(sig(pool_out.squeeze(-1)+self.offset)+1e-5)),dim=-1)
            logdet = logdet - torch.sum(torch.log(sig(self.s)+1e-5) * self.mask)
            return input_rev,logdet

class ISDP(nn.Module):
    def __init__(self, num_channels):
        super(ISDP, self).__init__()
        self.c=num_channels
        self.convq1=torch.nn.Parameter(torch.randn([num_channels,num_channels,1,1]),requires_grad=True)
        self.s = torch.nn.Softmax(dim=-1)
        self.convk1=torch.nn.Parameter(torch.randn([num_channels,num_channels,1,1]),requires_grad=True)
        self.register_parameter("offset",nn.Parameter(torch.ones([1,1,1])*1.01))
        self.register_parameter("scale",nn.Parameter(torch.ones([1,1,1])*10))
    def forward(self, input: torch.Tensor, logdet=0, reverse=False, permute=False):
        if not reverse:
            p = input.shape[-1]**2
            inp = rearrange(input) #get patches
            mask = checkerboard
            inp_rev = reverse_rearrange(inp*mask)
            q1= Conv2d(inp_rev,self.convq1)#Convq
            k1= Conv2d(inp_rev,self.convk1)#Convk
            full_inp_q1 = rearrange(q1) #get patchwise features:Queries
            full_inp_k1 = rearrange(k1) #get patchwise features:Keys
            attn_mask = checkerboard
            attn = (self.s((torch.matmul(full_inp_q1, full_inp_k1.permute(0, 2, 1))/self.scale)))*attn_mask #Compute attention
            id=torch.eye(attn.shape[-1]).cuda()*self.offset # identity matrix to ensure proper logdet computation
            logdet_sdp = torch.slogdet(attn+id)[1]*p*(p//2)*self.c
            logdet = logdet + logdet_sdp
            out_attn= torch.matmul(attn+id, inp * (1 - mask))
            out= out_attn * (1 - mask) + inp * mask
            output=reverse_rearrange(out)
        else:
            p = input.shape[-1]**2
            out = rearrange(input)
            mask = checkerboard
            if permute:
                mask=1-mask
            rev = out * mask
            rev_rearrange = reverse_rearrange(rev)
            q1= Conv2d(rev_rearrange,self.convq1)
            k1= Conv2d(rev_rearrange,self.convk1)
            full_inp_q1_rev = rearrange(q1) # get patchwise features:Queries
            full_inp_k1_rev= rearrange(k1) # get patchwise features:Keys
            attn_mask = checkerboard
            attn = (self.s((torch.matmul(full_inp_q1_rev, full_inp_k1_rev.permute(0, 2, 1))/self.scale)))*attn_mask
            id = torch.eye(attn.shape[-1]).cuda()* self.offset # identity matrix to ensure proper logdet computation
            logdet_sdp = torch.slogdet(attn + id)[1] * p * (p // 2) * self.c
            logdet = logdet - logdet_sdp
            attn_inv= torch.inverse(attn+id)
            out_attn = torch.matmul(attn_inv, out * (1 - mask))
            output= out_attn * (1 - mask) + out * mask
            output=reverse_rearrange(output)
        return output,logdet

```

Figure 15: Pseudo code of the proposed iMap and iSDP modules.

Hence, it is valuable to optimize the aggregation of the two complementary types of attention (i.e., first- and second-order attentions) for real-world scenarios. To this end, one of the most promising directions is to exploit neural architecture search algorithms over them.